S.T. Yau High School Science Award

Research Report

The Team

Name of team member: YuanZhi Wang
School: St. Michaels University School
City, Country: Victoria，Canada

Name of team member: N/A
School: N/A
City, Country: N/A

Name of team member: N/A
School: N/A
City, Country: N/A

Name of supervising teacher: Jordan Tessarolo
Job Title: Head of Science
School/Institution: St. Michaels University School
City, Country: Victoria，Canada

Title of Research Report

[Development of an Autonomous Cleaning Robot Based on Helical Propulsion for Sandy Beach Benthic Organism Protection and Its Ecological Restoration Efficacy]

Date

[7/13/2026]

Development of an Autonomous Cleaning Robot Based on Helical Propulsion for Sandy Beach Benthic Organism Protection and Its Ecological Restoration Efficacy

YuanZhi Wang

Abstract

Sandy beaches provide important habitats for benthic organisms, but conventional cleaning machines often damage sediment structures while removing surface waste. This conflict between cleaning efficiency and ecological protection motivates the development of a low-disturbance autonomous cleaning system.

This study presents an autonomous beach-cleaning robot integrating helical propulsion, visual recognition, and active waste collection. An Archimedes screw-based propulsion mechanism is designed to generate lateral shear force rather than vertical compaction, enabling movement on soft sand with reduced habitat disturbance. The robot combines YOLOv8-based micro-litter recognition, ROS2 autonomous control, LiDAR-assisted mapping, and a soft-tooth collection mechanism to identify and remove small beach debris.

Experimental results show that the optimized helical structure achieves effective propulsion with a 30 mm pitch and 45° helix angle. Compared with a tracked mechanism, the proposed robot reduces sand surface damage depth from 28.3 mm to 11.8 mm (58% reduction) while improving waste collection efficiency from 81.9% to 94.2%. The recognition module achieves accuracies of 89%, 94%, and 82% for cigarette butts, plastic bottle caps, and paper scraps, respectively. The integrated system achieves a cleaning success rate of 92.5%.

Keywords: Helical propulsion; Autonomous cleaning robot; Sandy beach ecosystem; YOLOv8; ROS2; Ecological protection.

Acknowledgement

Foremost, I would like to express my sincere gratitude to my teacher, Mr. Tessarolo, the Head of Science, for his generous support, assistance and encouragement during this research. I couldn’ t imagine finishing all of these series of experiments and making this kind of progress without his support. I would also like to thank my classmates and friends, for their suggestions, comments and help during the research.

AI Use Statement: This article only underwent grammar correction and language polishing using Chat GPT before the formal submission of the paper.

Commitments on Academic Honesty and Integrity

We hereby declare that we

1. are fully committed to the principle of honesty, integrity and fair play throughout the competition.
2. actually perform the research work ourselves and thus truly understand the content of the work.
3. observe the common standard of academic integrity adopted by most journals and degree theses.
4. have declared all the assistance and contribution we have received from any personnel, agency, institution, etc. for the research work.
5. undertake to avoid getting in touch with assessment panel members in a way that may lead to direct or indirect conflict of interest.
6. undertake to avoid any interaction with assessment panel members that would undermine the neutrality of the panel member and fairness of the assessment process.
7. observe the safety regulations of the laboratory(ies) where we conduct the experiment(s), if applicable.
8. observe all rules and regulations of the competition.
9. agree that the decision of YHSA is final in all matters related to the competition.

We understand and agree that failure to honour the above commitments may lead to disqualification from the competition and/or removal of reward, if applicable; that any unethical deeds, if found, will be disclosed to the school principal of team member(s) and relevant parties if deemed necessary; and that the decision of YHSA is final and no appeal will be accepted.

(Signatures of full team below)

x Yuanzhi Wang
Name of team member:

x (Jordan Tessarolo)
Name of supervising teacher:

Contents

1. Introduction 1
1.1. Research Background: Micro-Litter and Sandy-Beach Benthic Organisms 1
1.2. Research Problem: The Conflict Between Cleaning Efficiency and Habitat Disturbance 2
1.3. Research Objective and Main Argument 3
2. Rationale for Selecting a Low-Disturbance Propulsion Scheme 4
2.1. Comparison of Three Mobility Mechanisms 4
2.2. Slip-Sinkage Problems of Conventional Propulsion Methods 5
2.3. Reasons for Selecting Helical Propulsion 6
3. System Design of the Autonomous Cleaning Robot 7
3.1. Overall System Configuration 7
3.2. Helical Propulsion Mechanism 9
3.3. Litter Collection Mechanism 11
3.4. Perception, Control and Power Components 13
3.5. System Operating Process 14
4. Experimental Analysis of Motion and Cleaning Performance 14
4.1. Layered Structure of the Experimental Analysis 14
4.2. Effects of Helical Structural Parameters on Propulsion Performance 15
4.3. Propulsion Performance Under Different Sand Conditions and Speeds 16
4.4. Validation of Whole-Robot Motion Performance 17
4.5. Comparative Validation of Helical and Tracked Mechanisms 18
5. YOLOv8-Based Micro-Litter Recognition and Autonomous Perception 20
5.1. Role of Visual Recognition in the System 20
5.2. Recognition Training Process 21
5.3. Real-Time Tracking Performance 23
5.4. Training Convergence and Classification Results 24
6. Integrated System Analysis and Innovation 26
6.1. Complete Logic From Problem to Solution 26
6.2. Integrated Interpretation of Experimental Results 26
6.3. Three System Innovations 27
7. Conclusion 27
8. Summary of Results 28
9. Future Work 29
References 30
Appendix A Main Hardware Components of the System 32

1. Introduction

1.1. Research Background: Micro-Litter and Sandy-Beach Benthic Organisms

Sandy beaches are not only busy coastal spaces for human activities, but also provide living environments for various benthic organisms. Benthic organisms participate in the material and nutrient cycling processes in the nearshore ecosystem and are an important component in maintaining the ecological functions of the beach [1]. Once microplastics enter the coastal environment, they may be ingested by low-nutrient-level marine animals and cause physical effects [2]; the leachate and chemical components of cigarette butts may also have toxic effects on marine and freshwater fish [3]. Moreover, in the intertidal mudflat environment, the distribution and foraging behavior of wading birds can reflect the bottom ecological conditions and changes in food resources [4]. Therefore, the problem of garbage cleanup on the surface of the beach primarily stems from the need to protect the living environment of benthic organisms.

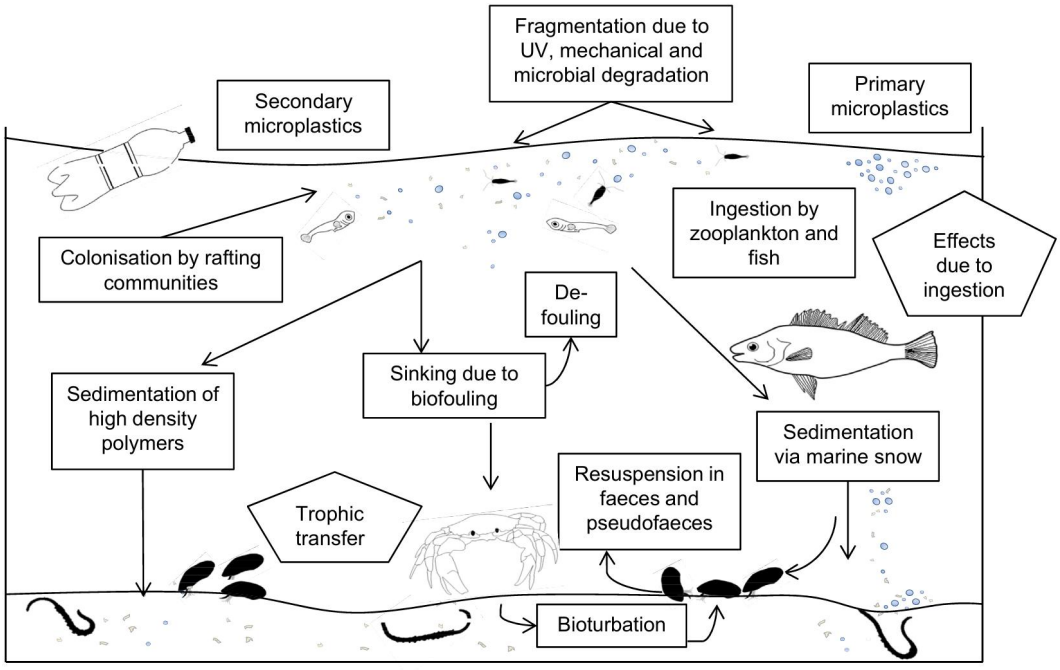


Figure 1.1 Schematic of Microplastic Transport and Interactions with Marine Organisms [8]

As shown in Figure 1.1, microplastics can include primary microplastics and secondary microplastics formed under the influence of ultraviolet rays, mechanical forces, and microbial degradation, and they can affect the marine environment through deposition, biological attachment, ingestion and food chain transmission [2,5,6,7]. In the figure, plastic fragments, plankton, fish and benthic environments are linked together, indicating that small-scale

garbage located on sandy surfaces and in nearshore waters is not isolated but will enter environmental processes related to biological activities. Therefore, the objects of this study are not the general surface waste, but the microplastics in fragile habitats.

Plastic waste in the beach environment can undergo aging and fragmentation processes to form smaller-scale plastic particles, and these particles can establish connections with the benthic habitat through deposition or biological ingestion, etc. [5, 6, 7]. As shown in Figure 1.2, this mechanism explains why this study needs to focus on the identification and low-disturbance collection of micro-waste.

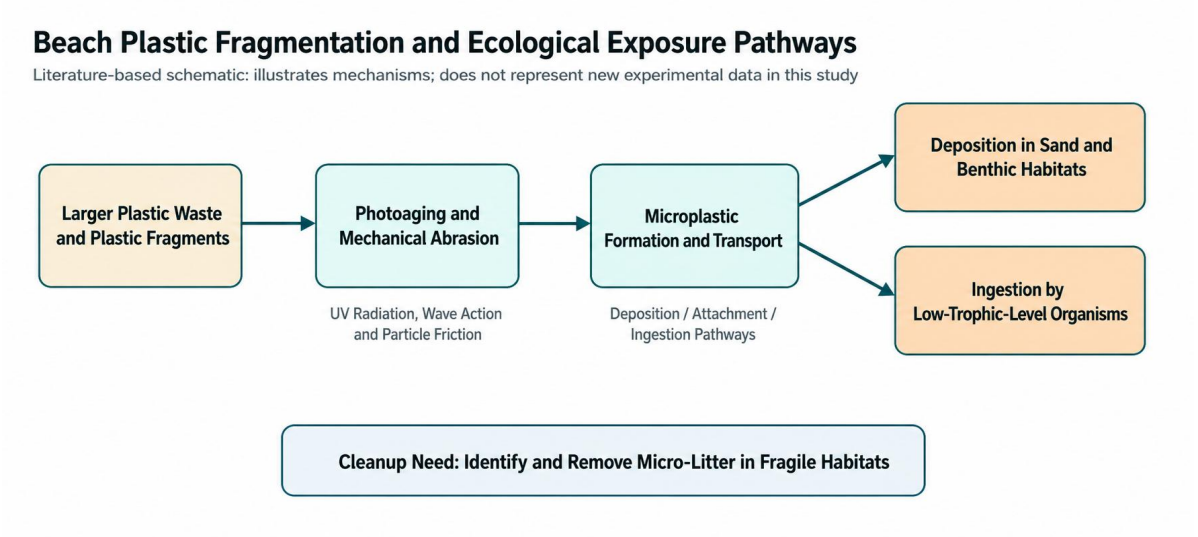


Figure 1.2 Schematic of Beach Plastic Fragmentation and Ecological Exposure Pathways [2,5,6,7]

1.2. Research Problem: The Conflict Between Cleaning Efficiency and Habitat Disturbance

For the beach cleaning task, the removal of garbage does not mean that the problem has been properly resolved. The sandy beach ecosystem is subjected to various types of human disturbance pressures [9]; studies on beach cleaning methods further indicate that mechanized cleaning may have an impact on the beach ecological environment [10]. Traditional heavy machinery, while removing surface garbage, crushes fragile habitats because large cleaning devices need to bear, move and sieve on the soft sand surface. The reason is that the large cleaning devices require the sand surface to bear, move and sieve, and the moving process itself changes the structure of the surface sand. As shown in Figure 1.3, conventional large cleaning equipment has larger working mechanisms and higher loads, and its operation mode has tension with the meticulous and low-disturbance operation required for the protection of benthic organisms.



Figure 1.3 Conventional Large-Scale Beach-Cleaning Equipment

Therefore, the research question of this paper is: How to develop an autonomous robot system that can identify and collect micro garbage on the beach, while minimizing the disturbance to the sand structure during the movement and collection process? This question encompasses two inseparable target dimensions: The first is task effectiveness, meaning the robot needs to identify the target garbage and complete the collection; the second is environmental adaptability, meaning the robot needs to maintain a low ground pressure and minimal subsidence on the soft sand surface. Only when both are simultaneously achieved within the same system can the cleaning plan serve the protection of benthic organisms and ecological restoration.

1.3. Research Objective and Main Argument

Regarding the above issues, the sole overall objective of this paper is to develop a beach autonomous cleaning robot that combines spiral low-disturbance movement, micro garbage identification, and active collection. This robot aims to complete garbage removal while reducing the disturbance to the bottom-dwelling organisms on the sandy surface. To achieve this goal, the system adopts three interrelated technical components: replacing traditional wheeled or tracked propulsion with spiral propulsion; deploying the YOLOv8 visual recognition system to detect micro garbage; integrating ROS2, SLAM, path planning, and a front collection mechanism to complete autonomous cleaning.

The entire text unfolds along the same argument chain. Chapter 2 compares wheeled, tracked, and spiral mechanisms to explain why spiral propulsion is adopted; Chapter 3 describes the robot structure, perception control, and collection execution as how they constitute a complete system; Chapter 4 analyzes the low-disturbance movement and

collection performance layer by layer through parameters, sand surfaces, the entire vehicle, and mechanism control experiments; Chapter 5 analyzes the recognition results of YOLOv8 for micro garbage; Chapter 6 integrates the three aspects of movement, perception, and ecological protection; Chapter 7 and Chapter 8 respectively present the research conclusions and future work.

2. Rationale for Selecting a Low-Disturbance Propulsion Scheme

2.1. Comparison of Three Mobility Mechanisms

Whether robots can complete tasks in sandy environments depends primarily on the interaction mode between their moving mechanisms and the soft substrate. Wheeled, tracked, and spiral mechanisms exhibit significant differences in terms of ground pressure, subsidence depth, shear effects, sand surface mobility, and ecological impacts. This comparison is not a general mechanical assessment divorced from the task, but rather examines whether the robots can move and whether the moving process reduces disturbances.

Table 2.1 Comparison of Mobility Mechanisms on Sandy Ground

Feature	Wheeled Mechanism	Tracked Mechanism	Helical Mechanism
Ground Pressure	High	Moderate	Ultra-low (approx. 1.6 kPa)
Sinkage Depth	Severe (>15 mm)	Significant	Minimum (<5 mm)
Shear Effect	Localized	Severe	Gentle
Mobility on Sand	Poor	Moderate	Excellent
Ecological Impact	Destructive	Traumatic	Refined and low-disturbance

As shown in Table 2.1, the ground pressure of the wheeled mechanism is high and the subsidence is severe. Although the tracked mechanism reduces the single-point pressure, its shear effect is still quite intense. The screw mechanism, on the other hand, corresponds to ultra-low ground pressure, small subsidence, gentle shear, and excellent sand surface movement capability. Therefore, in this study, the screw mechanism is adopted as the mobile solution for ecological protection: this mechanism not only needs to push the robot forward, but also needs to support the cleaning operation with minimal sand surface disturbance.

2.2. Slip-Sinkage Problems of Conventional Propulsion Methods

As shown in Figure 2.1, the wheeled mechanism may exhibit more pronounced sliding-sinking behavior on soft ground as the sliding ratio increases. In the sand cleaning task, such sinking not only affects the forward efficiency of the robot but also causes the wheel to disturb the surface layer of the sand more deeply, resulting in structural collapse and high sinking.

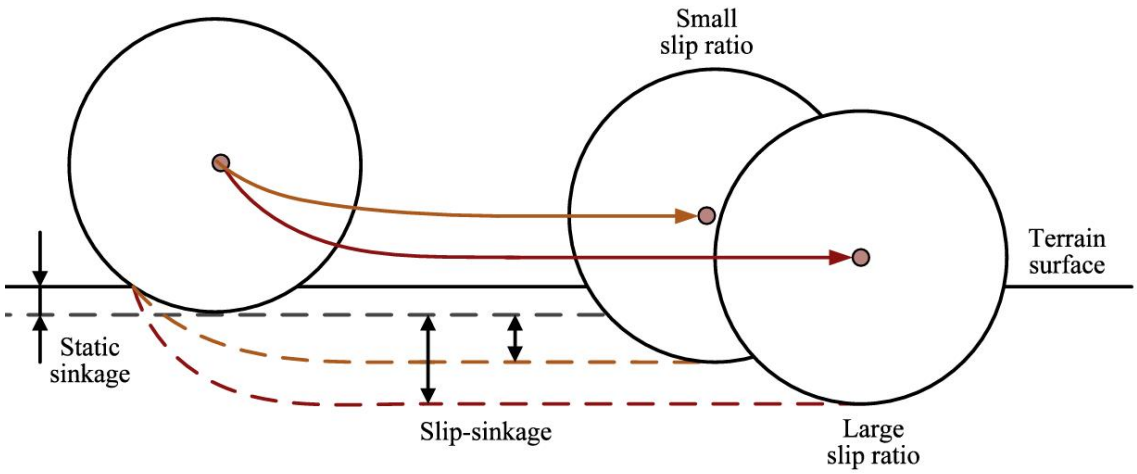


Figure 2.1 Schematic of the Slip-Sinkage Mechanism of Wheels on Soft Ground

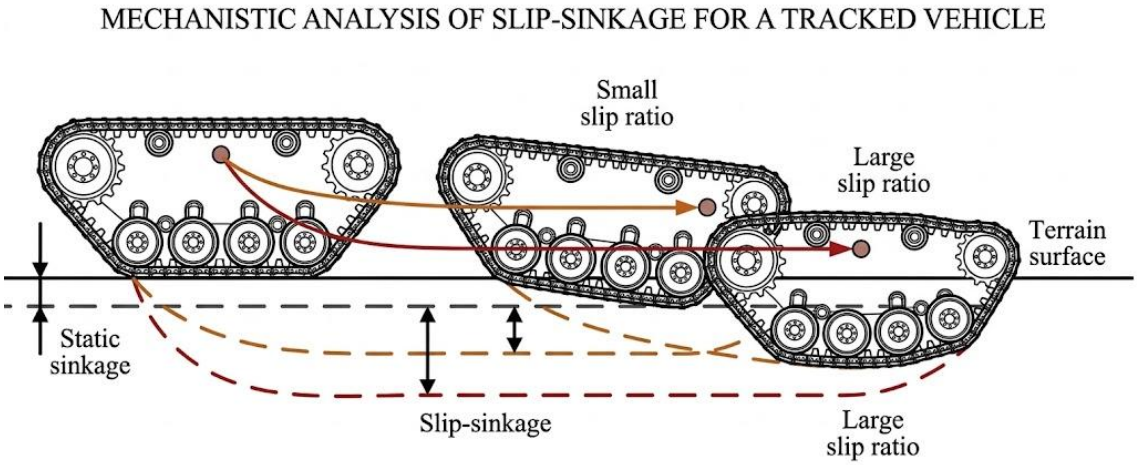


Figure 2.2 Schematic of the Slip-Sinkage Mechanism of Tracks on Soft Ground

The crawler mechanism expands the contact area with the ground, but it may still cause severe shearing and surface trauma. As shown in Figure 2.2, the crawler will also exhibit variations in subsidence under different sliding conditions; when the crawler pushes the sand forward or to the side, the surface structure will be disturbed. Therefore, the common limitation of the wheeled and crawler schemes does not lie in the inability to clean, but rather

in the fact that their movement methods in soft sand surfaces and the goal of low disturbance protection are not completely consistent.

2.3. Reasons for Selecting Helical Propulsion

The common drawbacks of wheeled and tracked systems can be summarized as the "dumper effect": the systems tend to push the sand forward rather than smoothly traverse the sand surface, thereby increasing energy consumption and disturbing the habitat. To address this issue, the helical propulsion generates propulsion force through the interaction between the helical blades and the sand, and converts the "vertical compaction" into "lateral shear propulsion" by using Archimedes' spiral shear drive. The research on Archimedes' spiral propulsion in non-paved terrain vehicles and soft soil mobile robots provides an engineering basis for the selection of the propulsion scheme in this paper [11, 12].

For cleaning tasks, the robot needs to move to the location where the garbage is scattered; for protection tasks, the robot's movement path should not introduce obvious surface damage. The spiral mechanism has four advantages: low disturbance movement, superior traction on soft sandy ground, precise garbage extraction, and optimized energy efficiency. Therefore, choosing spiral propulsion is a specific technical path to achieve low-disturbance autonomous movement.

Compared with the movement mode that mainly relies on vertical bearing and may drive the movement of the surface sediment, the Archimedes spiral mechanism generates propulsion force through the shear effect between the drum and the soft substrate. This mechanism is consistent with the research on spiral propulsion in non-paved terrain vehicles and soft soil mobile robots [11, 12]. As shown in Figure 2.3, this figure is used to illustrate the theoretical basis for the selection of the low-disturbance propulsion route in this paper, and is not presented as new experimental results.

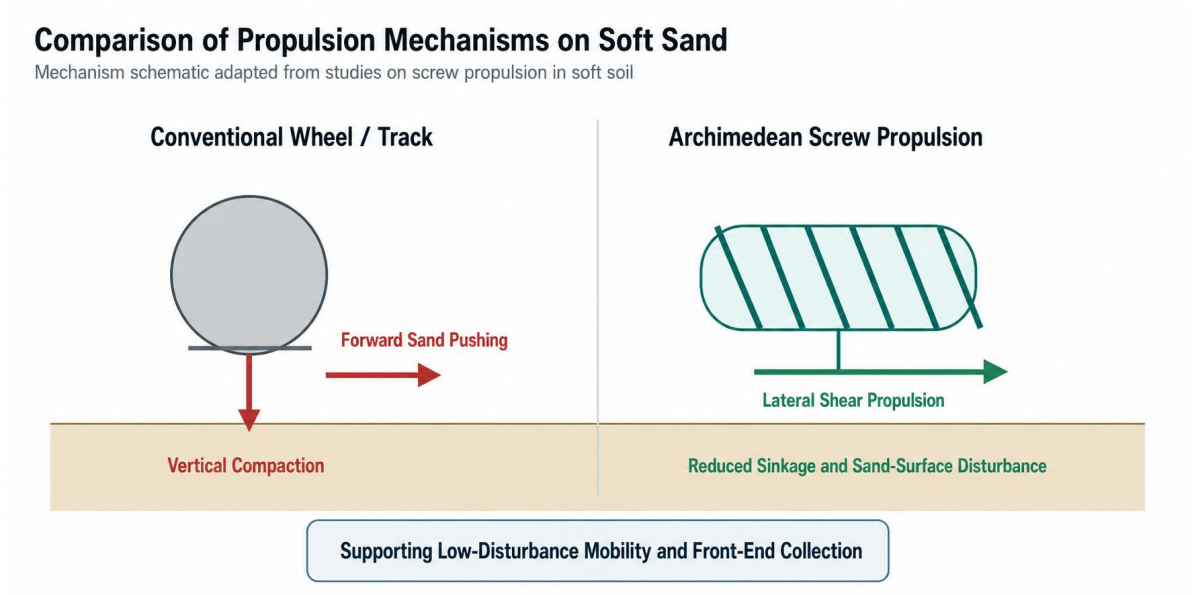


Figure 2.3 Schematic of the Interaction Between Archimedean Screw Propulsion and Soft Sand [11,12]

3. System Design of the Autonomous Cleaning Robot

3.1. Overall System Configuration

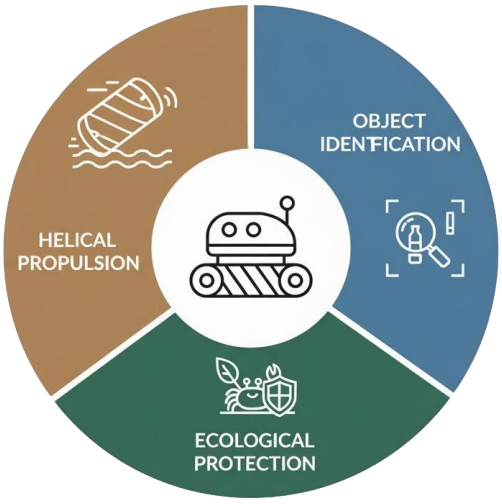


Figure 3.1 Three Core System Functions: Helical Propulsion, Object Recognition and Ecological Protection

After determining that the spiral propulsion is the mode of movement, the system must also complete the tasks of garbage detection, path execution and garbage extraction to form a complete autonomous cleaning robot. The system functions consist of three parts: spiral propulsion, object recognition and ecological protection. As shown in Figure 3.1, these three

functions form a closed loop around the robot: the spiral propulsion supports low-disturbance operations, object recognition locates micro-garbage, and ecological protection reflects the system's control over the disturbance on the sand surface.

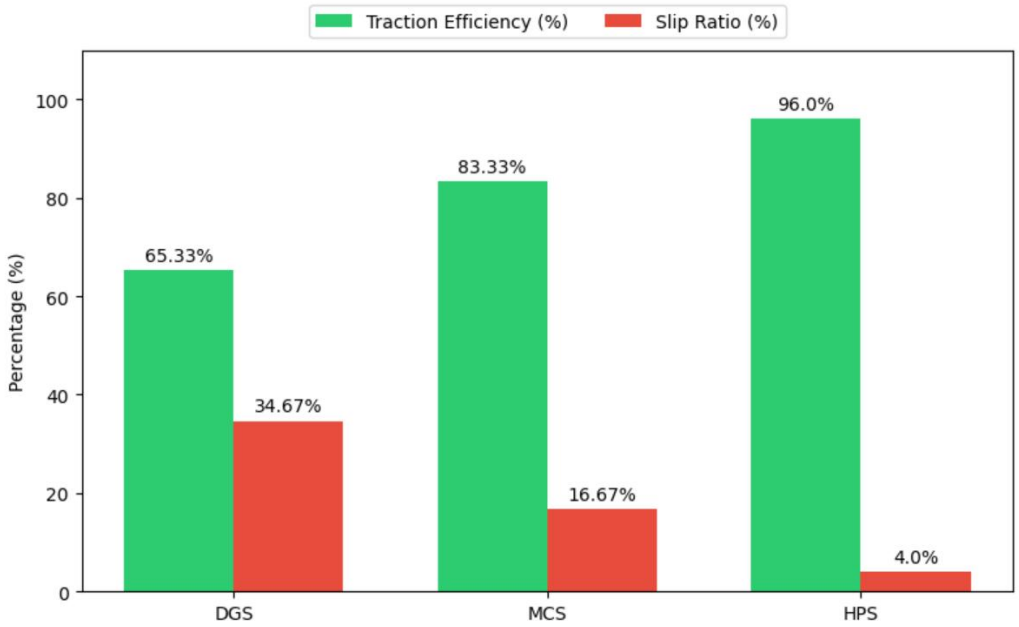


Figure 3.2 Three-Dimensional Design of the Helical-Propulsion Autonomous Cleaning Robot

As shown in Figure 3.2, the three-dimensional design of the robot arranges the spiral propulsion components on both sides of the vehicle body, installs the garbage collection structure at the front, and reserves the control, perception and power supply parts on the upper part. From this structure, it can be seen that propulsion and collection are not two separate devices, but are jointly installed on the same platform, enabling the robot to approach and handle garbage during its movement.

The three-dimensional plan was further realized as a physical prototype. As shown in Figure 3.3, when the prototype runs on the sand surface, the spiral propulsion modules on both sides of the vehicle body directly interact with the sand surface, while the front end of the vehicle body is responsible for garbage contact and collection. This prototype provides a physical basis for structural parameter testing, vehicle performance testing, and comparison of spiral/track systems.



Figure 3.3 Physical Prototype of the Helical-Propulsion Autonomous Cleaning Robot

3.2. Helical Propulsion Mechanism

The spiral propulsion mechanism is the core of the system in this paper for achieving low-disturbance movement. This mechanism realizes dynamic adaptation on the soft sand surface through Archimedes spiral shear drive. The left and right spiral drums are driven by motors, and built-in Hall encoders are used for speed feedback. As shown in Figure 3.4, the unilateral propulsion mechanism is composed of a motor, mounting bracket, shaft components, transmission structure, and spiral drum; this configuration enables the driving force to act on the spiral drum through the transmission components.

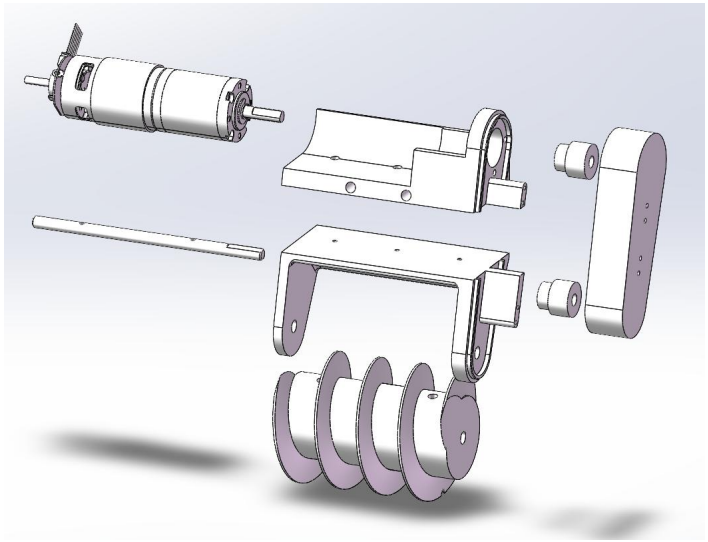


Figure 3.4 Exploded View of the Helical Propulsion Mechanism

As shown in Figure 3.5, the assembled single-side propulsion unit integrates the motor, bracket and spiral drum into an integrated module. As shown in Figure 3.6, the physical test

wheel has a distinct spiral blade structure. The blades directly contact the sand body during operation and provide propulsion. The three figures successively present the implementation method of the spiral propulsion unit from structural disassembly, assembly composition to physical state, and also provide a structural basis for the analysis of pitch, helix angle and length experiments in Chapter 4.

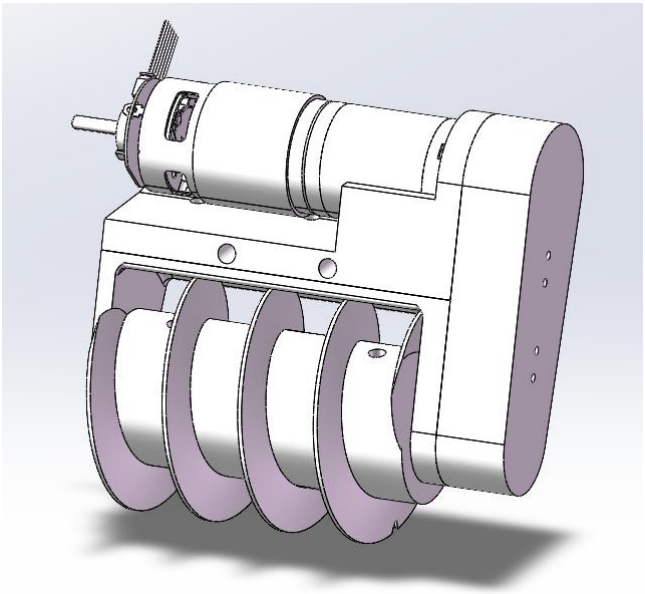


Figure 3.5 Assembly of the Helical Propulsion Unit

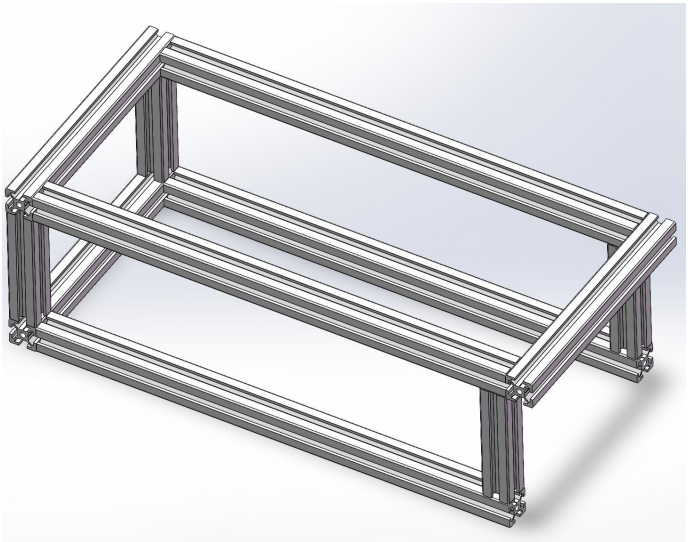


Figure 3.6 Physical Test Drum for Helical Propulsion

For a single-head ideal spiral drum, the blade shape can be described by the geometric relationship between the pitch and the helix angle. Let the effective radius of the drum be r, the axial advancing pitch of a single rotation be P, and the helix angle be α, then:

$$P = 2\pi r \tan \alpha \tag{3-1}$$

Equation (3-1) is used to explain the structural relationship between pitch P, helix angle α and the size of the drum. In this paper, the selection of 30 mm pitch and 45° helix angle still relies on the actual experimental results presented in Chapter 4. This geometric formula does not replace the measured and optimized conclusions in the sand surface.

Based on the above structural relationship, the connection between the rotation of the drum and the movement of the robot can also be described using the simplest displacement model. If the spiral drum rotates N complete circles, and in ideal conditions it moves one pitch P in the forward direction with each rotation, then the theoretical displacement $S_{t\hbar}$ is:

$$S_{t\hbar} = NP \tag{3-2}$$

If the rotational speed of the drum is n (r/min) and the movement time is t (s), then the number of rotations can be expressed as N = nt/60, thereby obtaining the same ideal displacement relationship:

$$S_{t\hbar} = \frac{Pnt}{60} \tag{3-3}$$

There is slippage and loosening of sand grains on the actual surface, so the actual displacement is usually less than the theoretical displacement. The effective advancement degree can be represented by the correction coefficient k, and it can be described simply as follows:

$$S_{act} = kS_{t\hbar}\ ,\quad 0 < k \leq 1 \tag{3-4}$$

Equations (3-2) to (3-4) illustrate that pitch, rotational speed and working time will increase the theoretical propulsion distance, while the sliding caused by the soft sand surface will result in a reduction of the actual moving distance.

3.3. Litter Collection Mechanism

Low-disturbance movement solves the problem of how the robot reaches the garbage location, while the garbage collection structure is responsible for performing the actual cleaning action. The front-mounted active soft tooth collection rollers are driven by a motor and are used to sweep the garbage into the internal collection box; the vibration motors are placed near the collection box or the soft tooth rollers to assist in separating sand particles from garbage and preventing blockages. As shown in Figure 3.7, the collection structure includes a driving device and a front rotating component, enabling it to come into contact with the sandy surface target.

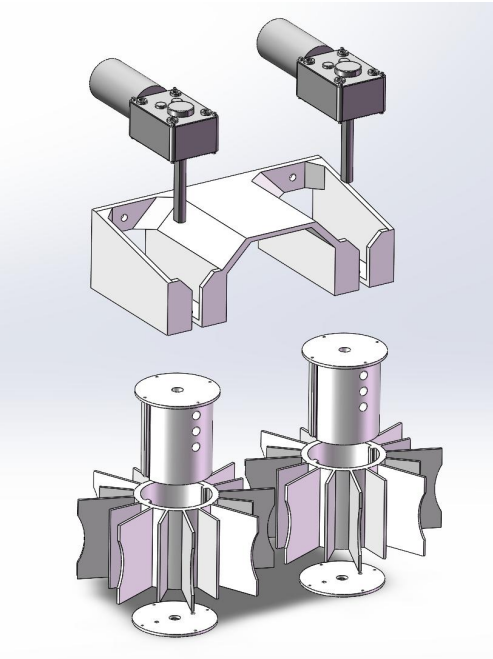


Figure 3.7 Exploded View of the Front Litter-Collection Structure

As shown in Figure 3.8, the collection structure comes into contact with the bottle-shaped garbage in the sand surface working scene, demonstrating the garbage extraction function of the robot's front-end device. This structure forms a clear division of labor with the spiral propulsion: the spiral drum is used for low-disturbance movement and positioning, the front-end collection mechanism is used to incorporate the target object into the collection area, and the vibration auxiliary function is used to reduce the risk of blockage caused by sand particles mixing in.

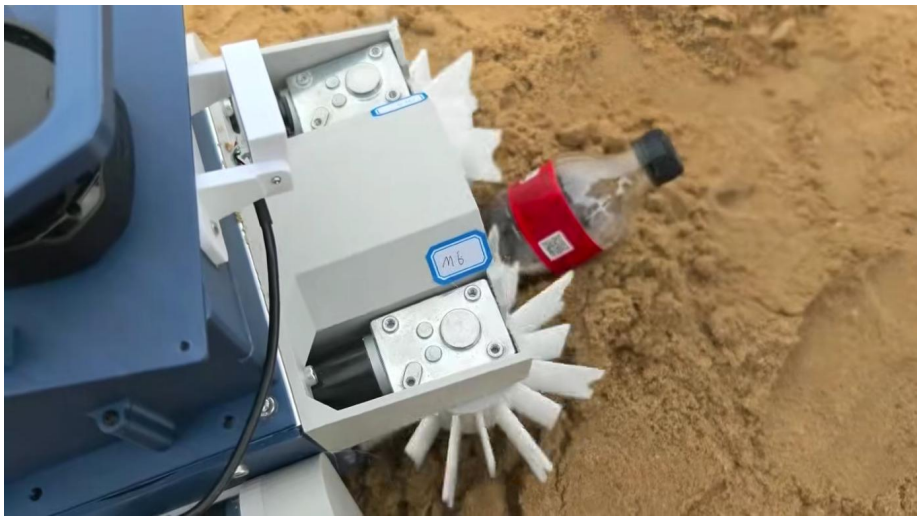


Figure 3.8 Front Litter-Collection Structure in Operation

3.4. Perception, Control and Power Components

The autonomous cleaning system needs to connect the mechanical structure with the information processing function. The open-source robot operating system ROS provides a software framework basis for the organization of the sensing, mapping, planning and control modules [13], and the SLAM research provides a method background for the robot to simultaneously perform positioning and environmental mapping [14]. The main controller of this system runs ROS2, YOLOv8 inference, SLAM mapping and path planning, responsible for processing sensor data and sending control commands to the actuators. The camera acquires images of the beach scene, providing input for YOLOv8 to identify micro garbage such as cigarette butts and plastics; the single-line LiDAR is used for real-time SLAM mapping, obstacle detection and positioning, and provides two-dimensional point cloud data.

In the execution and power supply section, the motor driver receives the PWM signals sent by the Raspberry Pi, and drives four 24 V spiral propulsion motors and two 24 V collection motors respectively; the main power supply provides 24 V direct current to the motor driver, the voltage reduction module and other integrated modules. The synchronous belt and synchronous pulley are responsible for transmitting power, the aluminum profiles are used to construct a lightweight and high-strength chassis support frame, and the linear axes are used to bear the rotational support of the spiral drum or the supporting structure. The functions, components and their roles in the cleaning task are shown in Table 3.1.

Table 3.1 Components and Functions of the Autonomous Cleaning System

System Stage	Components	Role in the Cleaning Task
Perception Input	Camera; Single-line LiDAR	Identify micro-litter and provide mapping, obstacle-detection and localization information.
Computation and Decision-Making	Raspberry Pi 5; ROS2; YOLOv8; SLAM; Path Planning	Process environmental information and generate motion and cleaning commands.
Low-Disturbance Mobility	Helical Drums; Motors; Hall Encoder	Provide propulsion on soft sand and return speed feedback.
Waste Extraction	Soft-tooth Roller; Vibration Motor; Collection Bin	Sweep waste into the bin and assist sand separation.
Drive and Support	Motor Driver; Buck Module; 24 V Supply; Timing Belt; Aluminum Profile; Linear Shaft	Supply power to actuators and form the mechanical foundation of the robot.

3.5. System Operating Process

The robot's operation process follows a continuous sequence of "identification - planning - approaching - collection". The camera first captures the image of the sandy surface, and YOLOv8 detects garbage such as cigarette butts, plastic bottle caps, and paper scraps in the image; the single-line LiDAR simultaneously provides information for mapping the environment, obstacle detection, and positioning. The main controller organizes the recognition, SLAM, and path planning modules in the ROS2 platform, and generates movement commands based on the location of the garbage and environmental information. The classic heuristic minimum cost path search research provides a basic method reference for the robot's path selection problem [15]; this paper does not claim to specifically adopt a certain individual algorithm, but regards path planning as a part of the system's autonomous execution chain.

Subsequently, the drive unit controls four helical propulsion motors to enable the robot to approach the target area with minimal disturbance. The front soft teeth collection wheels sweep the garbage into the collection box, and the vibration motor assists in separating the sand particles from the garbage. This process forms a complete system with each structure and module: the perception stage answers "what to clean", the planning and propulsion stage answers "how to reach", the collection stage answers "how to remove", and the low-disturbance helical characteristic runs through the entire process to protect the sandy environment where benthic organisms can move freely.

4. Experimental Analysis of Motion and Cleaning Performance

4.1. Layered Structure of the Experimental Analysis

The verification of motion and cleaning performance is carried out in an order from local to overall, and from design to application. Firstly, the pitch, helix angle and drum length are compared to select the structural parameters suitable for spiral propulsion; secondly, different sand surface conditions and driving speeds are compared to analyze the influence of external media on the traction efficiency and slip rate; subsequently, the vehicle performance verification examines the actual speed, slip and steering performance of the robot under changes in motor speed; finally, the comparison of the spiral and track mechanisms summarizes the motion stability, sand surface damage and garbage collection effect into the same task for comparison.

Therefore, this chapter is analyzed in the order from structure to task: The spiral robot first achieves effective propulsion at the parameter level, then tests its movement performance under varying sand surface conditions, subsequently verifies controllable driving at the vehicle level, and finally compares and contrasts the damage to the sand surface and the garbage collection rate through the tracks.

4.2. Effects of Helical Structural Parameters on Propulsion Performance

The effect of the spiral propulsion mechanism is closely related to the geometric parameters. In this paper, pitch P, helix angle α and drum length L are taken as the comparison variables, and the displacement changes under different schemes are used to represent the propulsion effect. As shown in Figure 4.1, the three sets of curves respectively present the displacement results over time under the conditions of pitch, helix angle and length.

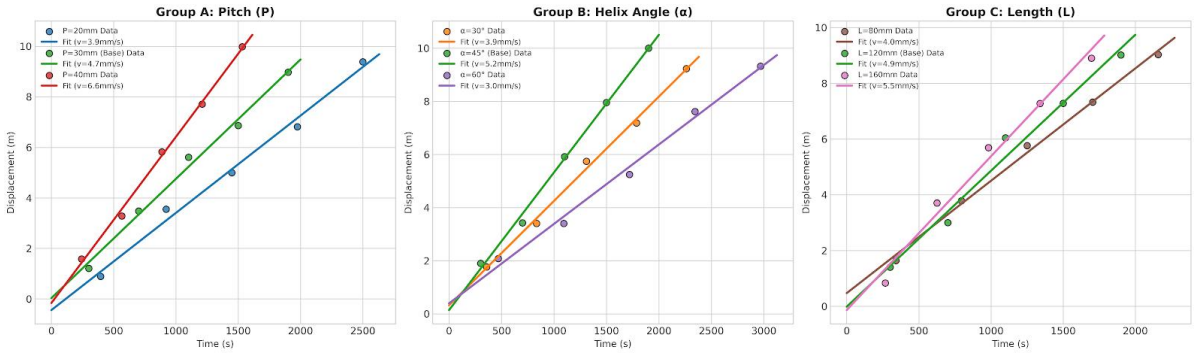


Figure 4.1 Comparison of Propulsive Displacement Under Different Pitches, Helix Angles and Drum Lengths

In the pitch comparison, a higher pitch can increase the speed, but it will cause shear failure. Therefore, 30 mm is chosen as the optimal pitch. This judgment takes into account both the propulsion displacement and the sand body effect: the propulsion structure needs to have sufficient displacement capacity, but its parameters cannot only be based solely on speed, because excessive shear action will damage the integrity of the sand body structure.

In the comparison of helix angles, 45° can maximize efficiency, while 60° will cause excessive excavation and thrust loss. This result indicates that the helix angle affects the interaction mode between the drum and the sand body: in this system, the motion effect corresponding to 45° can better balance propulsion and ground interaction. The length comparison shows that increasing L can increase the contact area and stability, and effectively suppress slippage. The results of these three types of parameters together form the structural basis for the subsequent vehicle design.

4.3. Propulsion Performance Under Different Sand Conditions and Speeds

After the parameters of the screw mechanism are selected, its actual performance is still affected by the condition of the sand surface. This paper compares the traction efficiency and slip rate under different conditions of sand surface compactness. As shown in Figure 4.2, the high compactness sand surface (HPS) corresponds to the highest traction efficiency and the lowest slip rate. The efficiency reaches 96.0% and the slip rate is only 4.0%; this is related to its higher sand surface shear strength.



Figure 4.2 Traction Efficiency and Slip Ratio Under Different Sand-Surface Conditions

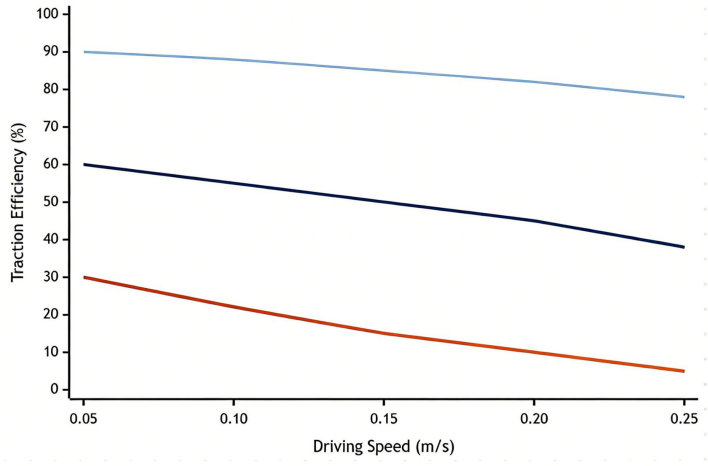


Figure 4.3 Effects of Driving Speed on Traction Efficiency Across Sand Conditions

The influence of sand surface conditions is also reflected in the process of speed variation. As shown in Figure 4.3, as the driving speed increases, the traction efficiency of the sand surface shows a downward trend; among them, the loose sand surface is more sensitive to speed changes. This means that the low disturbance and traction capabilities

demonstrated by the spiral propulsion need to be understood in conjunction with the actual substrate conditions: the same mechanism can achieve higher efficiency on a more compact ground, but will face efficiency attenuation on a looser sand surface or at higher speeds.

This group of experiments linked the institutional design with the actual beach environment. The parameter experiments answered the question of what kind of structural combination the spiral drum should adopt, while the sand surface and speed experiments explained how the selected structure would perform under varying external conditions. Together, these two aspects illustrate that the spiral propulsion is not merely a structural design that operates under fixed conditions, but rather a motion capability plan tailored to the characteristics of the sandy medium.

4.4. Validation of Whole-Robot Motion Performance

After the analysis of the individual advancement effect, this paper further conducts the verification of the vehicle performance. The complete robot is composed of a four-wheel helical drive system, so the actual movement of the vehicle will also be affected by factors such as particle medium resistance, slip coupling, and lateral sand pushing during the steering process. As shown in Figure 4.4, the vehicle verification presents the robot's performance under different motor input speeds in three aspects: forward speed response, slip and efficiency dynamics, and steering maneuverability.

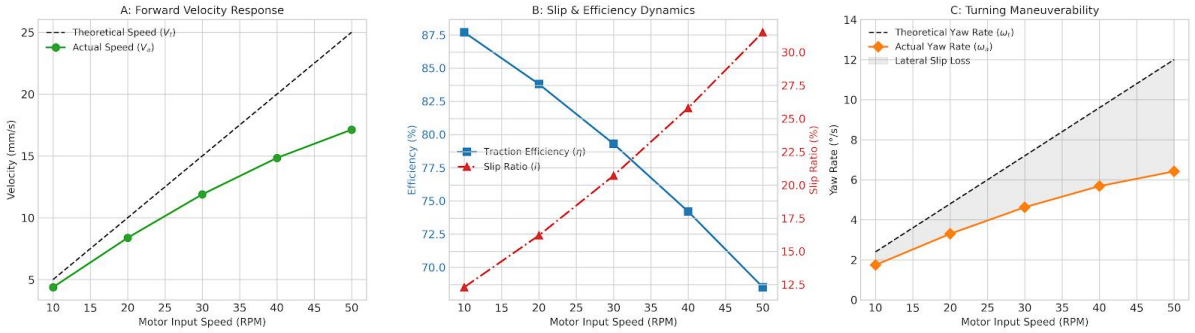


Figure 4.4 Whole-Robot Speed Response, Slip and Efficiency Dynamics, and Steering Maneuverability

The vehicle speed response can be analyzed by the difference between the theoretical propulsion speed and the actual moving speed. Under the ideal conditions of a single-head spiral drum without slippage, assuming the drum rotation speed is n (r/min), the theoretical linear speed v_{th} is:

$$v_{th} = \frac{Pn}{60} \tag{4-1}$$

Let the actual forward speed measured for the entire vehicle be v_{act}. Then the slip ratio s can be expressed as:

$$s = \frac{(v_{th} - v_{act})}{v_{th}} \times 100\% \quad (4\text{-}2)$$

To describe the degree of realization of the actual speed relative to the theoretical output, the motion realization rate η_v is defined. This quantity is obtained from the speed ratio and is used to explain the speed lag and slip variation; it does not directly replace the traction efficiency definition that might be adopted in the test diagram:

$$\eta_v = \frac{v_{act}}{v_{th}} \times 100\% = 100\% - s \quad (4\text{-}3)$$

Firstly, as the RPM increases, the actual driving speed shows a significant lag compared to the theoretical speed, reflecting the resistance loss of the four-wheel helical drive system in the granular medium. Secondly, the slip rate increases from 12.3% to 31.5% as the motor speed rises, while the traction efficiency decreases, indicating that the effective motion output is affected by slippage during high-speed operation. Finally, in the steering motion, due to the lateral pushing force limitation, the actual yaw angular velocity saturates at 6.42° /s at high rotational speeds.

The vehicle experiments have shown that the low-disturbance spiral propulsion system not only requires appropriate drum parameters, but also needs to take into account the relationship between speed, slip and steering in the actual motion state of the real robot. The experiments did not equate the maximum motor speed with the optimal operation state, but rather used phenomena such as speed lag, slip growth and steering saturation to illustrate the actual limitations in the operation of the entire machine.

4.5. Comparative Validation of Helical and Tracked Mechanisms

After completing the analysis of structural parameters, surface adaptability and vehicle dynamics, this paper conducts a direct comparison at the task level between the screw mechanism and the crawler mechanism. This comparison focuses on three aspects: whether the robot can complete the task on the sandy surface, how much surface impact is caused during the operation, and how much garbage the robot can collect. As shown in Figure 4.5, the comparison results include driving speed, success rate, sand excavation depth on the surface and garbage collection effect. The comparison results of the three key performance indicators are presented in Table 4.1.

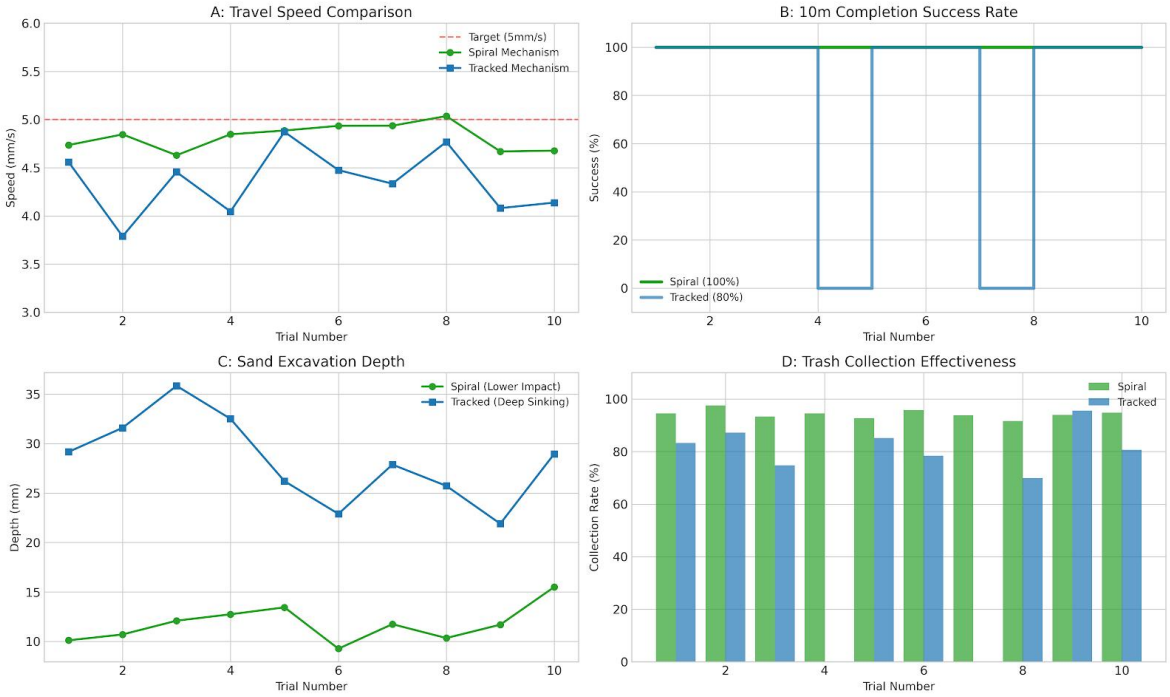


Figure 4.5 Comprehensive Performance Comparison Between Helical and Tracked Mechanisms

Table 4.1 Performance Comparison Between Helical and Tracked Mechanisms

Comparison Item	Helical Mechanism	Tracked Mechanism	Result Analysis
Environmental Adaptability Rate	100%	80%	The helical mechanism achieved a higher task-completion rate.
Sand-Surface Damage Depth	11.8 mm	28.3 mm	The helical mechanism reduced surface damage by 58%.
Waste Collection Rate	94.2%	81.9%	Stable helical operation achieved a higher collection rate.

The comparison of environmental adaptability rates shows that the screw mechanism achieved 100% in the test tasks, while the tracked mechanism achieved 80%; this result corresponds to the robot's ability to complete the sand surface cleaning route. In terms of the depth of sand surface damage, the 11.8 mm of the screw mechanism is 58% less than the 28.3 mm of the tracked mechanism, directly corresponding to the low disturbance design purpose of this paper. In terms of garbage collection rate, the screw mechanism reached 94.2%, higher than the 81.9% of the tracked mechanism, indicating that reducing surface influence did not come at the expense of giving up cleaning effectiveness.

The depth of sand surface damage can be directly used to quantify the degree of reduction in disturbance of the screw mechanism relative to the track mechanism. Let the

depth of sand surface damage of the track mechanism and the screw mechanism be d_t and d_h respectively, then the reduction rate R_d is:

$$R_d = \frac{(d_t - d_h)}{d_t} \times 100\% = \frac{(28.3 - 11.8)}{28.3} \times 100\% \approx 58.3\% \quad (4\text{-}4)$$

The calculation result of Equation (4-4) is consistent with the "reduction of 58%" reported in the text, thereby directly correlating the low disturbance design goal with the results of the control experiment.

Apart from the comparison of damage depth, the propulsion process can also be explained using the relationship between the base force and power. When the robot moves forward in a straight line at a nearly constant speed, the acceleration is close to zero, and the propulsive force F_T generated by the spiral is mainly used to overcome the resistance F_R of the sand to the robot:

$$F_T \approx F_R \quad (4\text{-}5)$$

If the actual forward speed of the robot is v_{act}, the propulsion output power P_m can be approximately estimated by multiplying the force by the speed:

$$P_m = F_T v_{act} \quad (4\text{-}6)$$

Equations (4-5) and (4-6) indicate that when the speed is the same, the smaller the sand surface resistance is, the less the thrust and power required to keep the robot moving forward; this is consistent with the design direction of this paper, which aims to reduce the disturbance from the sand surface and maintain smooth movement.

Thus, the control experiments yielded a set of interrelated results: The spiral mechanism can achieve a higher adaptation rate in the sand surface task, while also achieving lower sand surface damage and a higher garbage collection rate. This is also the main experimental basis for summarizing this scheme as a transition from powerful mechanical cleaning to precise ecological restoration.

5. YOLOv8-Based Micro-Litter Recognition and Autonomous Perception

5.1. Role of Visual Recognition in the System

Chapter 4 analyzes the spiral advancement and presents the collected results, demonstrating that the robot can move in sandy environments and perform cleaning actions. However, autonomous cleaning still requires answering a key question: How does the robot identify the micro garbage that needs to be cleaned? This paper uses YOLOv8 as the garbage recognition module, captures images of the sandy beach with a camera, recognizes

objects such as cigarette butts, plastic bottle caps, and paper scraps, and uses the recognition results to dynamically optimize the cleaning path to improve energy efficiency. The overview of the YOLO series architecture covers the evolution of real-time detection methods from YOLOv1 to YOLOv8, providing a methodological background for this paper to adopt YOLOv8 for lightweight target recognition [16].

Therefore, visual recognition is not an independent additional experiment separate from mechanical design, but rather a perception component within the overall system: the screw mechanism enables the robot to move with minimal disturbance, YOLOv8 enables the robot to locate the target garbage, ROS2 and path planning convert the recognition results into motion control, and the front collection mechanism ultimately completes the extraction.

5.2. Recognition Training Process

As shown in Figure 5.1, the YOLOv8 garbage recognition process starts with the input from the beach camera, and includes image data augmentation, labeled data set, visual feature extraction and fusion, training optimization, and real-time detection output. The end-to-end training process optimizes the information flow from the original image input to the detection output through a custom feature extraction and fusion module.

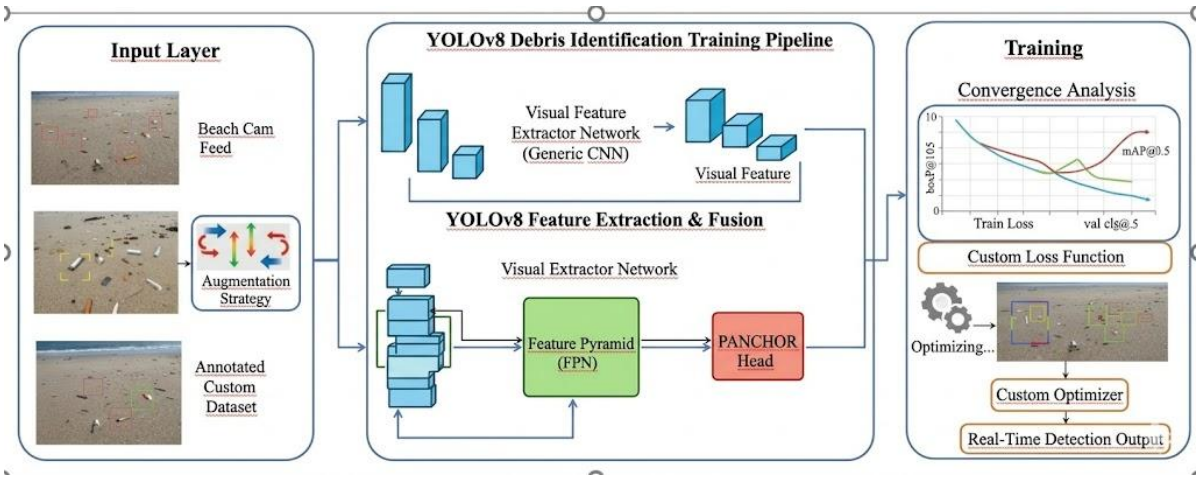


Figure 5.1 YOLOv8 Micro-Litter Recognition Training Process

This process is in line with the requirements of cleaning operations: the garbage targets in the sand surface are usually small in size and may be similar to the background texture. Therefore, the system needs to extract the target features from the input image and output the category and location. After the detection output is formed, the robot can perform approaches and collection actions around the identified object, allowing the perception results to enter the autonomous cleaning process.

The training process of the YOLOv8 detection model can be summarized as the joint optimization of localization, classification, and regression of bounding box distribution errors. Without altering the existing experimental results of this paper, the general form of its detection loss is [16]:

$$L_{det} = \lambda_{box} L_{box} + \lambda_{cls} L_{cls} + \lambda_{dfl} L_{dfl} \tag{5-1}$$

Among them, L_{box} represents the bounding box location loss, L_{cls} represents the class recognition loss, and L_{dfl} represents the distribution focus loss. λ_{box}, λ_{cls}, and λ_{dfl} are the corresponding weights. Equation (5-1) is used to describe the evaluation object of the training and validation loss convergence curves in Figure 5.3, without introducing additional training parameter values that are not reported in this paper.

To illustrate how the recognition module enters the actual program, the following presents a simplified YOLOv8 inference example. Here, best.pt represents the trained garbage recognition weight file, and the confidence threshold is set to 0.60, which is consistent with the threshold used in the confusion matrix analysis of this article.

Code 5.1 Example of YOLOv8 Beach-Litter Image Detection (Python)

```
from ultralytics import YOLO

model = YOLO("best.pt")
results = model.predict(source="beach_test.jpg", conf=0.60)

for box in results[0].boxes:
    cls_id = int(box.cls[0])
    score = float(box.conf[0])
    label = model.names[cls_id]
    print(label, round(score, 2))

results[0].save(filename="detect_result.jpg")
```

The program first loads the pre-trained model and reads the image to be detected. Then, it outputs the category name and confidence level of each detected object. Finally, it saves the result image with the detection boxes. The robot can further transmit the position of the detection boxes to the path planning and collection control module to achieve the connection from recognition to cleaning.

5.3. Real-Time Tracking Performance

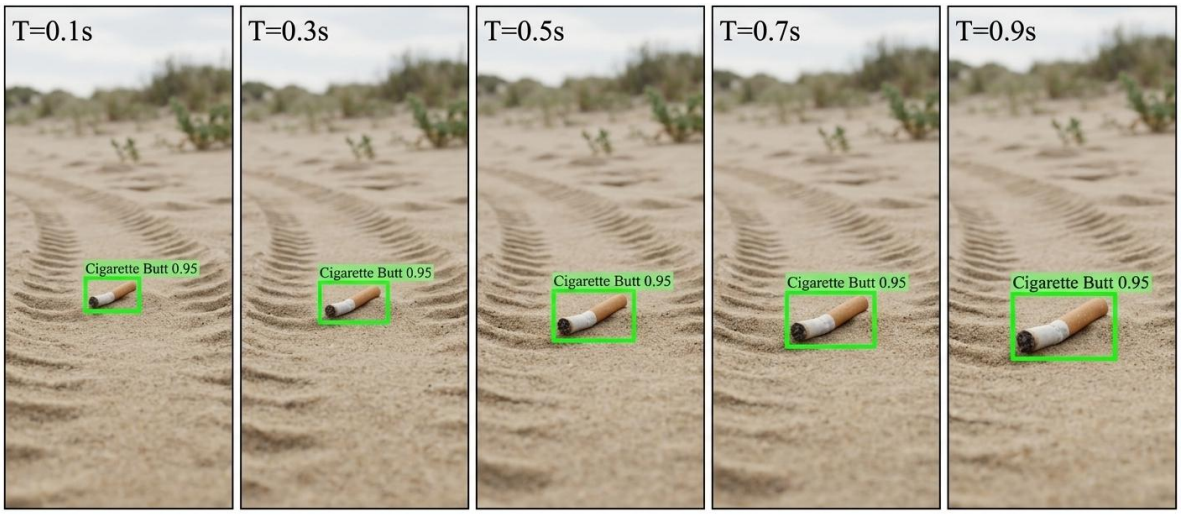


Figure 5.2: Evolution of the Perception System's Robustness on Deformable Terrain. **(b)** Continuous temporal tracking sequence: Stability of 'Cigarette Butt' detection amidst simulated helical propulsion oscillations.

Figure 5.2 Consecutive-Frame Tracking Sequence for a Cigarette-Butt Target

The visual recognition system not only needs to detect garbage in a single image, but also needs to maintain target tracking during the robot's movement. As shown in Figure 5.2, cigarette butt targets are all marked with detection boxes in consecutive time frames; in the sequence from T = 0.1 s to T = 0.9 s, the system continuously displays the corresponding confidence levels, indicating that it can maintain stable micro-garbage tracking during the movement.

The continuous tracking results have a direct correspondence with the operation process of the spiral-propelled robot. During the robot's movement, the position between the camera and the garbage target will continuously change; if the detection cannot remain stable, the subsequent path adjustment and collection actions will be difficult to be executed continuously. The time series shown in Figure 5.2 is thus used to illustrate that the recognition module can serve the cleaning task in motion.

5.4. Training Convergence and Classification Results

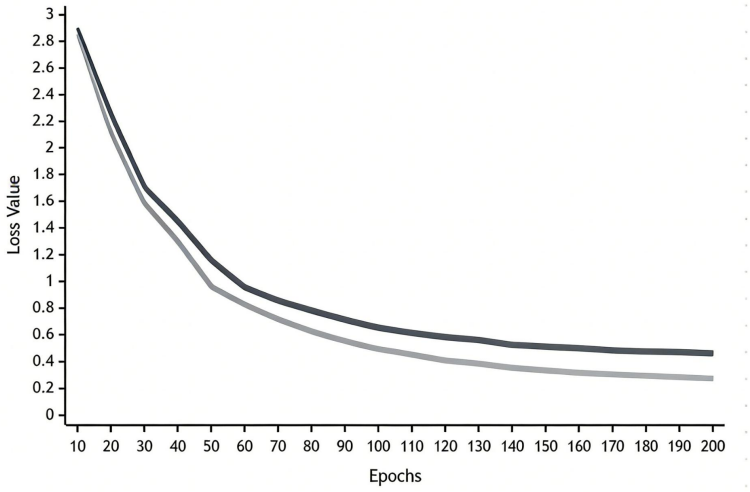


Figure 5.3 YOLOv8 Training and Validation Loss Convergence Curves

This paper analyzes the recognition performance through the convergence curves of training and validation losses, the P-R curves, and the confusion matrices. As shown in Figure 5.3, the loss during the training process shows a stable downward trend with each round, and the evolution of the loss and performance indicators reflects the effectiveness of the recognition structure.

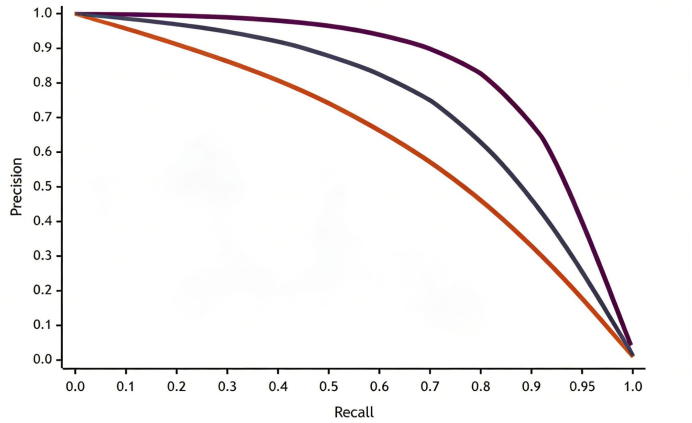


Figure 5.4 Precision-Recall (P-R) Curves for Different Litter Classes

As shown in Figure 5.4, the Precision-Recall (P-R) curves for different garbage categories are used to illustrate the model's performance in the relationship between precision and recall, and are employed to evaluate the reliability of the robot's autonomous identification in complex environments. The P-R curves and the loss curves respectively

present the performance of the YOLOv8 module from the training evolution and detection result perspectives.

In object detection, the matching degree between the predicted bounding box B_p and the true annotated bounding box B_g can be represented by the Intersection over Union (IoU) metric:

$$IoU = \frac{|B_p \cap B_g|}{|B_p \cup B_g|} \tag{5-2}$$

After the detection matching is completed, the precision and recall defined by the P-R curve are as follows:

$$Precision = \frac{TP}{TP + FP}, \quad Recall = \frac{TP}{TP + FN} \tag{5-3}$$

Among them, TP represents the number of correct detections, FP represents the number of false detections, and FN represents the number of missed detections. When the confusion matrix is normalized based on the true category, the diagonal element of the ith type of spam can be explained by the category recall rate R_i:

$$R_i = \frac{TP_i}{TP_i + FN_i} \tag{5-4}$$

Therefore, the recognition rates of cigarette butts, plastic bottle caps and paper scraps in the subsequent sections can be correlated with the performance of each category of recalls; this article only explains the existing confusion matrix results and does not provide additional mAP or overall accuracy rate values that were not given in the original results.

At the confidence threshold of 0.6, the confusion matrix results are shown in Table 5.1. The proportion of cigarette butts correctly identified as cigarette butts is 89%, the proportion of plastic bottle caps correctly identified as plastic bottle caps is 94%, and the proportion of paper scraps correctly identified as paper scraps is 82%. Additionally, the background missed detection rates for the three types of garbage are 8%, 5%, and 14% respectively.

Table 5.1 Confusion Matrix Results at a Confidence Threshold of 0.60

True Class / Predicted Class	Cigarette Butt	Plastic Bottle Cap	Paper Scrap	Background (Missed Detection)
Cigarette Butt	89%	2%	1%	8%
Plastic Bottle Cap	1%	94%	0%	5%
Paper Scrap	3%	1%	82%	14%

The confusion matrix results enable the identification performance to be correlated with the actual cleaning objects: The system can identify three types of micro-waste, among

which the recognition rate of plastic bottle caps is the highest, followed by cigarette butts, and the recognition rate of paper scraps is relatively low. Combined with continuous time frame tracking, training convergence, and P-R curve analysis, the visual module provides perceptual support for the robot to autonomously identify garbage in sandy environments.

6. Integrated System Analysis and Innovation

6.1. Complete Logic From Problem to Solution

The logical starting point of this article's system is the ecological protection contradiction in beach cleaning: microplastics and cigarette butts need to be removed from the beach environment, but traditional heavy machinery may disturb the sand bodies where bottom-dwelling organisms live during the cleaning process. Therefore, the robot solution cannot only pursue the cleaning result, but also must respond to the low disturbance requirement in the movement mode. The spiral propulsion corresponds to this movement mode choice, YOLOv8 corresponds to the identification of micro garbage, the front soft teeth rollers and vibration-assisted structures correspond to garbage collection, and ROS2, SLAM and path planning organize perception and execution into an autonomous operation process.

This system relationship forms a complete argument chain: it moves the supporting autonomous garbage collection in a spiral with low disturbance, while reducing the disturbance to the sandy habitat. The comparison of the mechanism explains why the spiral propulsion was chosen, the system design explains how this choice was realized, the experimental analysis explains how it performed, and the visual recognition explains how the robot carried out the operation towards the specific garbage target.

6.2. Integrated Interpretation of Experimental Results

The helical parameter experiment first answered how the propulsion structure was formed: a 30 mm pitch was found to be the preferred parameter between speed and shear effects. A 45° helical angle achieved the highest efficiency. Increasing the length increased the contact area and stability. The sand surface experiment further answered how the mechanism worked under different substrates and speeds: the traction efficiency on HPS was 96.0%, the slip rate was 4.0%, and the traction efficiency decreased with the increase in speed, while the loose sand surface was more sensitive to changes.

The vehicle experiment extended the results of the individual units to the complete robot, indicating that the slip rate increased from 12.3% to 31.5%, the traction efficiency decreased, the actual speed lagged behind, and the yaw angular velocity saturated at 6.42°/s at high RPM. The control experiment further unified the movement ability with the cleaning target:

the screw mechanism achieved 100%, 11.8 mm, and 94.2% results in terms of environmental adaptability, sand surface damage, and collection rate, corresponding to 80%, 28.3 mm, and 81.9% for the tracked mechanism.

The perception experiment answers how the robot discovers the objects to be cleaned: YOLOv8 can track cigarette butts in consecutive time frames and provides recognition results of 89% for cigarette butts, 94% for plastic bottle caps, and 82% for paper scraps. Thus, the movement, collection, and recognition results collectively correspond to the two requirements of low-disturbance operation and micro garbage cleaning.

6.3. Three System Innovations

Table 6.1 Three Innovations and Their Roles in the System Logic

Innovation Aspect	Technical Content	Role in the System Logic
Helical Propulsion	Implements Archimedean screw shear drive, converting vertical compaction into lateral shear propulsion and adapting dynamically to soft sandy substrate.	Addresses low-disturbance mobility on sand.
Ecological Protection	Optimizes contact geometry and reduces surface-subsidence disturbance by 58% compared with a conventional tracked mechanism, minimizing impacts on fragile coastal micro-ecosystems.	Links mobility performance to the protection goal for benthic habitats.
Object Recognition	Deploys visual perception and edge detection for real-time, high-accuracy litter recognition, dynamically optimizing the cleaning path for energy efficiency.	Provides target-perception input for autonomous cleaning.

As shown in Table 6.1, the three innovations are not separate technical labels but rather a series of interrelated system capabilities that are connected around the task of beach cleaning: The spiral propulsion enables the platform to operate on the soft sand surface, ecological protection emphasizes the reduction of disturbance to the sand surface caused by this operation mode, and object recognition enables the robot to autonomously complete the cleaning of specific micro garbage facing the specific micro garbage.

7. Conclusion

This paper focuses on the contradiction between the cleaning of micro garbage on the beach and the protection of bottom-dwelling organisms' habitat on the sand surface. An autonomous cleaning robot based on a helical propulsion system has been developed. The system reduces the vertical compaction effect caused by the traditional propulsion method through Archimedes spiral shear drive. It forms an autonomous perception and control link

with cameras, YOLOv8, LiDAR, ROS2, SLAM and path planning, and completes garbage extraction with a front-mounted active soft tooth collection roller and vibration-assisted structure.

The above experiments support this system design at different levels: at the parameter level, a 30 mm pitch and a 45° helical angle correspond to the best propulsion performance; at the sand surface condition level, the traction efficiency on the HPS reaches 96.0%, and the slip rate is 4.0%; at the vehicle level, the experiment shows an increase in slip, a decrease in efficiency, and a saturation phenomenon of high-speed steering during the speed increase process; at the control level, the helical mechanism achieves 100% environmental adaptability, a sand surface damage depth of 11.8 mm, and a garbage collection rate of 94.2%, which are respectively superior to those of the tracked mechanism (80%, 28.3 mm, and 81.9%); at the perception level, the YOLOv8 recognizes cigarette butts, plastic bottle caps, and paper scraps at proportions of 89%, 94%, and 82%, respectively.

Based on the above system and results, this study has achieved a transformation from intensive mechanical cleaning to meticulous ecological restoration in the operation mode, and has verified the ability of the spiral system to maintain operational efficiency while reducing environmental impact. The comprehensive results of the system are CSR 92.5% and MCT 485 s, indicating that this system can be an engineering feasible solution for sustainable coastal management.

8. Summary of Results

The main experimental validation results and corresponding system capabilities are shown in Table 8.1.

Table 8.1 Summary of Experimental Validation Results

Validation Item	Key Result	Corresponding System Capability
Structural Parameters	30 mm pitch; 45 deg helix angle; increasing L improves contact area and stability.	Supports the selection of a low-disturbance helical propulsion structure.
Sand-Surface Adaptability	Traction efficiency of 96.0% and slip rate of 4.0% on HPS; efficiency decreases as speed increases.	Shows that mechanism performance depends on sand and speed conditions.
Whole-Robot Dynamics	Slip rate from 12.3% to 31.5%; yaw angular velocity saturates at 6.42 deg/s.	Reflects the operating characteristics of the complete four-drum helical system.
Mechanism Comparison	100% vs. 80%; 11.8 mm vs. 28.3 mm; 94.2% vs. 81.9%.	Demonstrates adaptability, low disturbance and collection performance together.
Object	Cigarette butt 89%; plastic bottle cap	Provides micro-litter recognition

Validation Item	Key Result	Corresponding System Capability
Recognition	94%; paper scrap 82%.	capability.
Overall Results	CSR 92.5%; MCT 485 s.	Represents overall cleaning-task performance.

9. Future Work

Based on the existing systems of spiral propulsion, visual recognition and overall cleaning, this paper proposes five subsequent directions: while expanding the operation range, improving the perception of complex environments, reducing energy consumption and enhancing ecological friendliness, continue to carry out systematic optimization for the cleaning of micro garbage on beaches and the protection of benthic environments. The specific subsequent directions and their connections with the existing systems are shown in Table 9.1.

Table 9.1 Proposed Directions for Future Work

Direction	Future Work	Connection to the Existing System
Multi-Robot Collaboration	Develop a distributed multi-agent architecture to enable synchronized cleaning over large areas and improve coverage efficiency.	Extends single-robot cleaning capability to larger operating areas.
Adaptive Perception	Improve model robustness under salt spray and complex illumination to increase micro-litter classification accuracy.	Extends the environmental adaptability of the YOLOv8 visual-recognition module.
Biodegradable Modules	Develop biodegradable collection containers to achieve an environmentally friendly closed-loop robot life cycle.	Further aligns the waste-collection structure with ecological protection.
Edge Optimization	Optimize on-board model deployment to reduce power consumption while maintaining recognition accuracy and extending endurance.	Improves Raspberry Pi-side efficiency and continuous operation capability.
Dynamic Avoidance	Introduce dynamic avoidance strategies for tidal changes and active marine organisms.	Makes autonomous navigation further serve habitat protection.

References

[1] Knox, G. A. (2000). The Ecology of Seashores. CRC Press.

[2] Wright, S. L., Thompson, R. C., & Galloway, T. S. (2013). The physical impacts of microplastics on marine organisms: A review. Environmental Pollution, 178, 483-492. https://doi.org/10.1016/j.envpol.2013.02.031.

[3] Slaughter, E., Gersberg, R. M., Watanabe, K., Rudolph, J., Stransky, C., & Novotny, T. E. (2011). Toxicity of cigarette butts, and their chemical components, to marine and freshwater fish. Tobacco Control, 20(Suppl 1), i25-i29. https://doi.org/10.1136/tc.2010.040170.

[4] Mathot, K. J., Piersma, T., & Elner, R. W. (2018). Shorebirds as Integrators and Indicators of Mudflat Ecology. In P. G. Beninger (Ed.), Mudflat Ecology (pp. 309-338). Springer International Publishing. https://doi.org/10.1007/978-3-319-99194-8_12.

[5] Andrady, A. L. (2011). Microplastics in the marine environment. Marine Pollution Bulletin, 62(8), 1596-1605. https://doi.org/10.1016/j.marpolbul.2011.05.030.

[6] Barnes, D. K. A., Galgani, F., Thompson, R. C., & Barlaz, M. (2009). Accumulation and fragmentation of plastic debris in global environments. Philosophical Transactions of the Royal Society B: Biological Sciences, 364(1526), 1985-1998. https://doi.org/10.1098/rstb.2008.0205.

[7] Cole, M., Lindeque, P., Halsband, C., & Galloway, T. S. (2011). Microplastics as contaminants in the marine environment: A review. Marine Pollution Bulletin, 62(12), 2588-2597. https://doi.org/10.1016/j.marpolbul.2011.09.025.

[8] FISH. Vast Ocean, Yet Unable to Hold Human Desire [EB/OL]. CECA, 2020-08-26 [2026-05-24]. https://www.sohu.com/a/415067946_99932376.

[9] Defeo, O., McLachlan, A., Schoeman, D. S., Schlacher, T. A., Dugan, J., Jones, A., Lastra, M., & Scapini, F. (2009). Threats to sandy beach ecosystems: A review. Estuarine, Coastal and Shelf Science, 81(1), 1-12. https://doi.org/10.1016/j.ecss.2008.09.022.

[10] Zielinski, S., Botero, C. M., & Yanes, A. (2019). To clean or not to clean? A critical review of beach cleaning methods and impacts. Marine Pollution Bulletin, 139, 390-401. https://doi.org/10.1016/j.marpolbul.2018.12.027.

[11] Villacrés, J., Barczyk, M., & Lipsett, M. (2023). Literature review on Archimedean screw propulsion for off-road vehicles. Journal of Terramechanics, 108, 47-57. https://doi.org/10.1016/j.jterra.2023.05.001.

[12] Nagaoka, K., Otsuki, M., Kubota, T., & Tanaka, S. (2010). Terramechanics-based propulsive characteristics of mobile robot driven by Archimedean screw mechanism on

soft soil. In 2010 IEEE/RSJ International Conference on Intelligent Robots and Systems (pp. 4946-4951). https://doi.org/10.1109/IROS.2010.5651010.

[13] Quigley, M., Gerkey, B., Conley, K., Faust, J., Foote, T., Leibs, J., Berger, E., Wheeler, R., & Ng, A. Y. (2009). ROS: an open-source Robot Operating System. ICRA Workshop on Open Source Software.

[14] Cadena, C., Carlone, L., Carrillo, H., Latif, Y., Scaramuzza, D., Neira, J., Reid, I., & Leonard, J. J. (2016). Past, Present, and Future of Simultaneous Localization and Mapping: Toward the Robust-Perception Age. IEEE Transactions on Robotics, 32(6), 1309-1332. https://doi.org/10.1109/TRO.2016.2624754.

[15] Hart, P. E., Nilsson, N. J., & Raphael, B. (1968). A Formal Basis for the Heuristic Determination of Minimum Cost Paths. IEEE Transactions on Systems Science and Cybernetics, 4(2), 100-107. https://doi.org/10.1109/TSSC.1968.300136.

[16] Terven, J., Córdova-Esparza, D. M., & Romero-González, J. A. (2023). A Comprehensive Review of YOLO Architectures in Computer Vision: From YOLOv1 to YOLOv8 and YOLO-NAS. Machine Learning and Knowledge Extraction, 5(4), 1680-1716. https://doi.org/10.3390/make5040083.

Appendix A Main Hardware Components of the System

The robot control, perception and power-supply systems consist of the main hardware components shown below. These figures correspond to the functional descriptions in Section 3.4 and provide a complete view of the autonomous cleaning robot configuration.

As shown in Figure A.1, the Raspberry Pi 5 is the robot's main controller. It runs ROS2, YOLOv8 inference, SLAM mapping and path planning, processes sensor data and sends control commands.



Figure A.1 Raspberry Pi 5 Main Controller

As shown in Figure A.2, the single-line LiDAR performs real-time SLAM mapping, obstacle detection and localization, providing two-dimensional point-cloud environmental information for the system.



Figure A.2 Single-Line LiDAR

As shown in Figure A.3, the camera captures beach-scene images and provides input for YOLOv8 recognition of cigarette butts, plastics and other micro-litter.



Figure A.3 Visual Recognition Camera

As shown in Figure A.4, the 24 V power supply is the robot's main energy source and supplies power to control and execution components such as the motor driver and buck converter.



Figure A.4 24 V Whole-Robot Power Supply